ELSEVIER

Palaeogeography, Palaeoclimatology, Palaeoecology 187 (2002) 61–82

PALAEO

www.elsevier.com/locate/palaeo

Coupled productivity and carbon isotope records in the southwest Pacific Ocean during the late Miocene–early Pliocene biogenic bloom

Katharine M. Grant [a,*], Gerald R. Dickens [a,b]

[a] *School of Earth Sciences, James Cook University, Townsville, Qld 4811, Australia*
[b] *Department of Earth Science, Rice University, Houston, TX 77005, USA*

Received 19 December 2001; received in revised form 12 July 2002; accepted 18 July 2002

Abstract

Biogenic components of sediment accumulated at high rates beneath frontal zones of the Indian and Pacific oceans during the late Miocene and early Pliocene. The $\delta^{13}C$ of bulk and foraminiferal carbonate also decreased during this time interval. Although the two observations may be causally linked, and signify a major perturbation in global biogeochemical cycling, no site beneath a frontal zone has independent records of export production and $\delta^{13}C$ on multiple carbonate phases across the critical interval of interest. Deep Sea Drilling Project (DSDP) site 590 lies beneath the Tasman Front (TF), an eddy-generating jetstream in the southwest Pacific Ocean. To complement previous $\delta^{13}C$ records of planktic and benthic foraminifera at this location, late Neogene records of $CaCO_3$ mass accumulation rate (MAR), Ca/Ti, Ba/Ti, Al/Ti, and of bulk carbonate and foraminiferal $\delta^{13}C$ were constructed at site 590. The $\delta^{13}C$ records include bulk sediment, bulk sediment fractions (<63 μm and 5–25 μm), and the planktic foraminifera *Globigerina bulloides*, *Globigerinoides sacculifer* (with and without sac), and *Orbulina universa*. Using current time scales, $CaCO_3$ MARs, Ca/Ti, Al/Ti and Ba/Ti ratios are two to three times higher in upper Miocene and lower Pliocene sediment relative to overlying and underlying units. A significant decrease also occurs in all $\delta^{13}C$ records. All evidence indicates that enhanced export production – the 'biogenic bloom' – extended to the southwest Pacific Ocean between ca. 9 and 3.8 Ma, and this phenomenon is coupled with changes in $\delta^{13}C$ – the 'Chron C3AR carbon shift'. However, $CaCO_3$ MARs peak ca. 5 Ma whereas elemental ratios are highest ca. 6.5 Ma; foraminiferal $\delta^{13}C$ starts to decrease ca. 8 Ma whereas bulk carbonate $\delta^{13}C$ begins to drop ca. 5.6 Ma. Temporal discrepancies between the records can be explained by changes in the upwelling regime at the TF, perhaps signifying a link between changes in ocean–atmosphere circulation change and widespread primary productivity.

Keywords: Late Neogene; productivity; Tasman Sea; New Zealand; Australia; carbon isotopes

1. Introduction

For more than 20 years, studies of upper Miocene and lower Pliocene marine sediment have encountered two observations that somehow re-

* Corresponding author. Tel.: +61-7-4781-4363; Fax: +61-7-4725-1501.
E-mail address: katharine.grant@jcu.edu.au (K.M. Grant).

0031-0182/02/$ – see front matter
PII: S0031-0182(02)00508-4

flect major perturbations in global biogeochemical cycling. First, sediment components linked to primary productivity in surface waters (e.g. $CaCO_3$, SiO_2, P) accumulated at very high rates beneath upwelling zones throughout the Indian and Pacific oceans (e.g. Van Andel et al., 1975; Peterson et al., 1992; Delaney and Filippelli, 1994; Farrell et al., 1995; Dickens and Owen, 1999) and perhaps the Atlantic Ocean (Diester-Haass et al., 2002). This widespread increase in export production, termed the 'biogenic bloom', relates to an elevated supply of nutrients to the ocean, a major redistribution of nutrients within the ocean, or both (Delaney and Filippelli, 1994; Farrell et al., 1995; Dickens and Owen, 1996, 1999; Hermoyian and Owen, 2001). Second, carbon isotope ($\delta^{13}C$) records of bulk carbonate and benthic and planktic foraminifera at many locations decrease by 0.5–1.0‰ (e.g. Keigwin, 1979; Vincent et al., 1980; Savin et al., 1981; Loutit et al., 1983; Keigwin et al., 1987; Müller et al., 1991). This change in the isotopic composition of water masses, often referred to as the 'Epoch 6' or 'Chron C3AR' carbon shift (Vincent et al., 1980; Müller et al., 1991), signifies a change in the marine carbon cycle, possibly because of variations in deep water circulation, carbon supply to the ocean, or both (see above references).

Although the biogenic bloom and Chron C3AR carbon shift may be causally related and hint at fundamental oceanographic differences from the Miocene to the Pliocene, there are three immediate problems with placing these phenomena into scenarios of late Neogene global change. First, absolute ages for isochronous datums have changed significantly over the last 15 years, especially in the late Miocene (cf. Berggren et al., 1985, 1995b). Many key records across the time interval of interest are therefore not calibrated to a similar or current time scale (Dickens and Owen, 1999). Second, the timing and magnitude of the Chron C3AR carbon shift is problematic. Whereas $\delta^{13}C$ records from benthic and planktic foraminifera exhibit an abrupt -0.5 to -1.5‰ shift before Chron 3An (e.g. Bender and Graham, 1981; Keigwin et al., 1987), the excursion appears gradually after Chron 3An in bulk carbonate records (Mead et al., 1991; Shackleton and Hall, 1995, 1997). Third, despite potential links between enhanced productivity and the Chron C3AR carbon shift (Vincent et al., 1980, 1985; Berger and Vincent, 1986; Dickens and Owen, 1994), no study has independently examined past productivity and $\delta^{13}C$ in multiple carbonate phases at the same location. Thus, timing relationships between the two phenomena have remained uncertain.

Deep Sea Drilling Project (DSDP) site 590 (31°10.02′S; 163°21.51′E) lies on the eastern flank of the Lord Howe Rise (Fig. 1), a topographic high of thinned continental crust in the central Tasman Sea between Australia and New Zealand (Willcox et al., 1980; Auzende et al., 2000). Located at a water depth of 1299 m, this site is bathed by Antarctic Intermediate Water (AAIW) whilst the overlying surface waters form the Tasman Front (TF), a region of eddy-induced mixing. Upper Miocene to lower Pliocene sediments beneath the TF show elevated linear sedimentation rates (LSRs) and a significant drop in the $\delta^{13}C$ of foraminifera (Elmstrom and Kennett, 1986; Kennett, 1986; Nelson, 1986). Thus, sediment at this site may be ideal for investigating the biogenic bloom and Chron C3AR carbon shift together. In this study, we supplement previous work beneath the TF with records of export production and $\delta^{13}C$ on multiple carbonate phases. By placing all information on a current and common time scale (Berggren et al., 1995a,b), we document timing relationships between the biogenic bloom and the Chron C3AR carbon shift in the southwest Pacific and then discuss possible explanations for both.

2. Site 590 in the Tasman Sea

2.1. Oceanographic setting

The TF (Fig. 1) manifests as an eastward 'zonal jet' between 152° and 173°E, connecting the East Australian Current (EAC) with the East Cape Current (ECC) northeast of New Zealand (Warren, 1970). Numerous eddies are associated with this frontal zone (Tilburg et al., 2001) and surface waters are characterized by an abrupt change in temperature and salinity (Heath, 1985). Scott

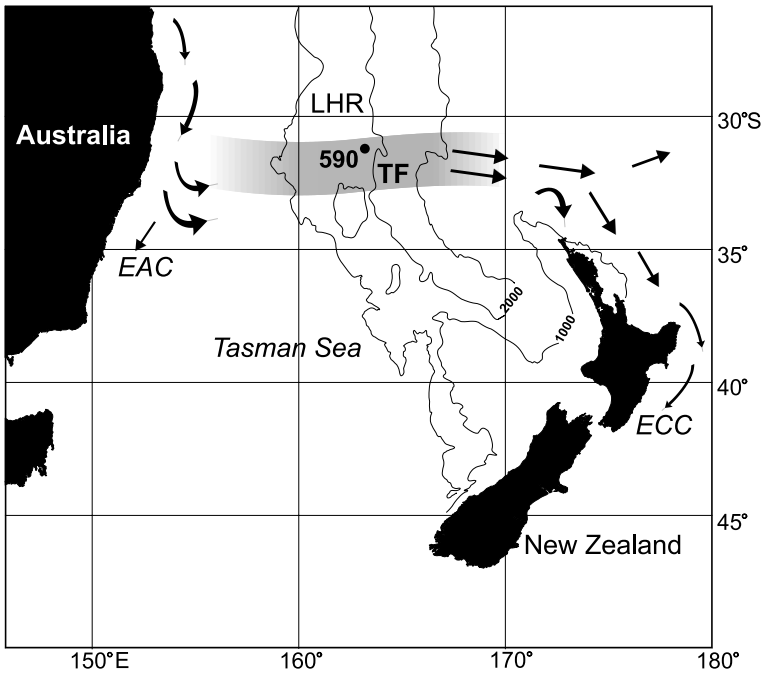

Fig. 1. Location map showing hydrography of the Tasman Front (TF), bathymetry of the Lord Howe Rise (LHR) and position of DSDP site 590. Depth contours are in meters; EAC = East Australian Current, ECC = East Cape Current.

(1981) observed seasonally elevated phytoplankton fluorescence within some eddies along the TF, and Comiso et al. (1993) found a positive correlation between seasonally elevated chlorophyll concentrations and the strength of Ekman upwelling in the Tasman Sea. A two-and-a-half-year analysis of the TF position (Mulhearn, 1987) has shown that it migrates between 30 and 38°S, but lies between 31 and 32.5°S for over half of the year. The TF may have migrated several degrees north during Pleistocene glacial intervals (Martínez, 1994; Kawagata, 2001). However, its average latitudinal position in the late Neogene was probably similar to that at present because the front is strongly influenced by the bathymetry of the Central Tasman Basin (Heath, 1985; Uddstrom and Oien, 1999) and this has been relatively stable for at least the past 15 million years (Myr) (Hayes and Ringis, 1973; Gaina et al., 1998). Site 590 is therefore ideally situated to monitor Miocene and Pliocene changes in oceanography at a frontal zone in the Southwest Pacific (Elmstrom and Kennett, 1986).

2.2. Previous observations at site 590

Upper Miocene to Holocene sediments at site 590 are dominantly white, foraminifera-bearing nannofossil ooze (Kennett et al., 1986) with carbonate concentrations generally exceeding 90% (Stein and Robert, 1986). Despite this uniform lithology, sedimentation rates (SRs) appear to have doubled in the late Miocene to early Pliocene (Nelson, 1986). This apparent increase in SRs coincided with a mixing of warm and cool-water planktic foraminifera assemblages and a drop in the $\delta^{13}C$ gradient between surface and deep-dwelling planktic foraminifera (Elmstrom and Kennett, 1986). The collective observations may reflect an increase in surface productivity caused by enhanced upwelling (Elmstrom and Kennett, 1986; Kennett and von der Borch, 1986). About 1–2 My before these oceanographic changes, planktic and benthic foraminifera $\delta^{13}C$ records also decrease by 1.5 and 0.9‰, respectively (Kennett, 1986). Thus, initial work at site 590 provides evidence for both the biogenic

Table 1
Age and depth of datums from holes 590A (*) and 590B used in this study

	Datum	Age (Ma)	Depth (mbsf)	Reference
N	FAD *Emiliania huxleyi*	0.26	3.80	a
N	LAD *Pseudoemiliania lacunosa* †	0.46	6.53	a
M	Base C1n	0.78	11.45	b
M	Top C1r.1n	0.99	15.50	b
M	Base C1r.1n	1.07	17.75	b
N	LAD *Calcidiscus macintyrei* ††	1.59	18.91	a
F	LAD *Globigerinoides fistulosus*	1.60	32.95*	a
M	Top C2n	1.77	33.20*	b
M	Top C2n	1.77	30.65	b
F	LAD *Globigerinoides obliquus extremus*	1.77	59.80*	a
M	Base C2n	1.95	35.75*	b
M	Base C2n	1.95	35.45	b
N	LAD *Discoaster broweri*	1.95	35.83	a
N	LAD *Discoaster pentaradiatus*[1]	2.51	45.43	a
N	LAD *Discoaster surculus*	2.57	46.21	a
F	FAD *Globorotalia truncatulinoides*	2.58	50.20*	a
M	Top C2An.1n	2.58	47.90*	b
M	Top C2An.1n	2.58	45.80	b
M	Base C2An.1n	3.04	62.50*	b
M	Base C2An.1n	3.04	57.65	b
F	LAD *Globorotalia multicamerata*	3.09	40.60*	a
F	LAD *Dentoglobigerina altispira*	3.09	69.40*	a
M	Top C2An.3n	3.33	70.08*	b
M	Top C2An.3n	3.33	60.60	b
F	FAD *Globigerinoides fistulosus*	3.33	59.80*	a
F	FAD *Globorotalia tosaensis*	3.35	80.95*	a
M	Base C2An.3n	3.58	81.20*	b
M	Base C2An.3n	3.58	70.35	b
F	LAD *Pulleniatina primalis*	3.65	80.95*	a
F	FAD *Globorotalia inflata*	3.70	100.15*	c
N	LAD *Reticulofenestra pseudoumbilica*[2]	3.75	87.61	a
N	FAD *Discoaster asymmetricus*	4.13	151.76	d
F	LAD *Globigerina nepenthes*	4.20	112.60*	a
F	LAD *Globorotalia cibaoensis*	4.60	127.00*	b
N	FAD *Ceratolithus rugosus*[3]	5.12	172.51	a
F	FAD *Globorotalia crassaformis* s.s.	5.20	167.35*	e
F	FAD *Globorotalia puncticulata*	5.20	191.35*	c
F	FAD *Globorotalia margaritae*	5.40	194.05*	e, f
N	LAD *Discoaster quinqueramus*	5.60	196.21	b
F	FAD *Globorotalia tumida*	5.60	162.55*	a
F	FAD *Pulleniatina primalis*	6.40	194.05*	b
F	FAD *Globorotalia conomiozea*	7.12	238.85*	b
N	FAD *Amaurolithus primus*[4] ‡	7.20	272.51	b
F	FAD *Globorotalia cibaoensis*	7.80	278.30*	b
N	FAD *Discoaster quinqueramus*	8.60	324.53	b
N	LAD *Discoaster hamatus*[5]	9.40	353.33	b
F	LAD *Globoquadrina dehiscens*	9.90	350.30	c, g
F	FAD *Neogloboquadrina acostaensis*	10.90	360.90	b
N	FAD *Discoaster kugleri*[6]	11.80	414.26	b
F	FAD *Globigerina nepenthes*	11.80	398.30	h

Ages for polarity chrons (M) and for first (FAD) and last (LAD) appearance datums of calcareous nannoplankton (N) and planktic foraminifera (F) are from (a) Berggren et al. (1995a), (b) Berggren et al. (1995b), (c) Morgans et al. (1996), (d) Shackleton et al. (1995), (e) Scott et al. (1990), (f) Srinivasan and Sinha (1992), (g) Wright and Vella (1988), (h) Ogg et al. (1998). *Pseudoemiliania lacunosa* is now commonly referred to as *Emiliania ovata* (†); similarly, *Cyclococcolithinia macintyrei* = *Calcidiscus macintyrei* (††) and *Ceratolithus primus* = *Amaurolithus primus* (‡). Datums used in the linear sedimentation rate model are numbered.

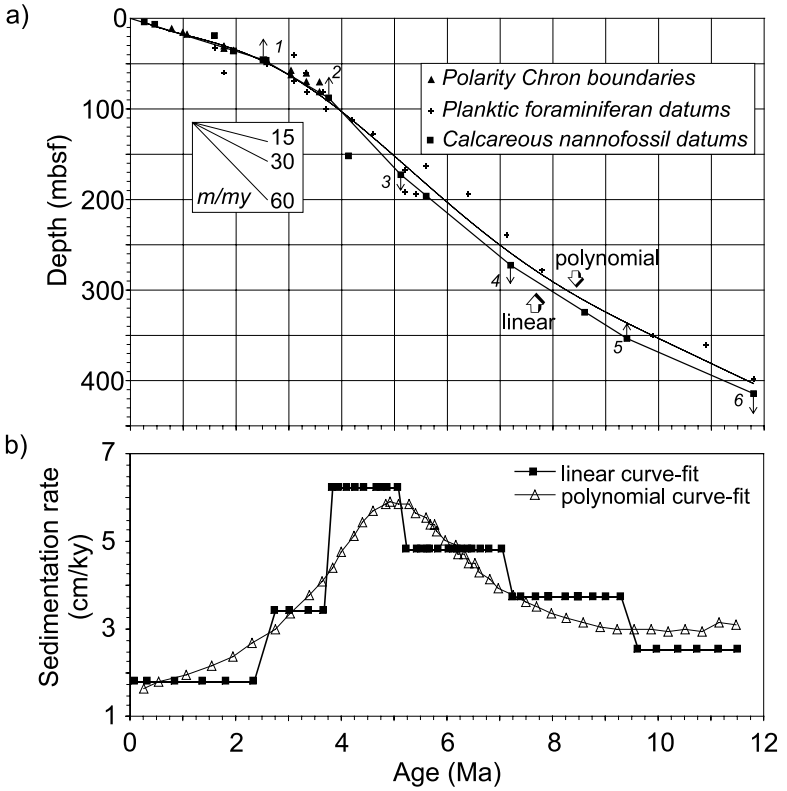

Fig. 2. (a) Age–depth model and SR curves for site 590. The linear SR curve is based on the datums numbered 1–6 (Table 1). The smoothed SR curve was determined by non-linear regression analysis using Engineering Equation Solver (EES) version 4.441, and is described by the polynomial equation: $y=(0.146+6.383e{-}2)x-(3.473e{-}4)x^2+(1.053e{-}6)x^3-(1.013e{-}9)x^4$. (b) Calculated SRs at site 590, using both the linear and polynomial curve-fitting methods.

bloom and the Chron C3AR carbon shift, with a temporal offset between the phenomena.

3. Revised age model and sedimentation rates

Numerous nannofossil, foraminifera, and polarity chron events have been identified at site 590 (Jenkins and Srinivasan, 1986; Lohman, 1986; Barton and Bloemendal, 1986). Previous workers (Kennett et al., 1986; Lazarus et al., 1992) have calibrated these datums to the time scale by Berggren et al. (1985), providing a detailed but now inaccurate age model. We assume that all datums have been correctly identified and positioned; we therefore have reassigned their ages (Table 1; Fig. 2) to the current and widely used time scale by Berggren et al. (1995a,b).

Typically SRs at a location are determined by fitting lines through age datums to obtain a stepped series of LSRs over time (Fig. 2). Although this approach is convenient, it often leads to artificial LSRs over certain depth intervals, especially where they change significantly. Polynomial fits through age datums provide an alternative means to estimate SRs. We have constructed SR curves at site 590 (Fig. 2) using both approaches and the revised age datums. With a stepped curve, LSRs increase from 2.7 cm/kyr at 11.8 Ma to a maximum of 7.1 cm/kyr at 5.3 Ma, remain high until 3.8 Ma, and then drop from 6.6 to 3.6 cm/kyr (Fig. 2). Alternatively, with a 'best-fit' fourth-order polynomial curve, SRs increase from 3.4 cm/kyr at 11.8 Ma to 6.7 cm/kyr at 4.9 Ma, and then gradually decline to 1.8 cm/kyr at 0.2 Ma (Fig. 2). Lower Pliocene sediment at site

Table 2
Carbonate concentrations and MARs at site 590

Sample (core, section, interval(cm))			Depth (mbsf)	Age_{LSR} (Ma)	Age_{POLY} (Ma)	$CaCO_3$ (%)	MAR_{LSR} $CaCO_3$ ($g/cm^2/kyr$)	MAR_{POLY} $CaCO_3$ ($g/cm^2/kyr$)
1H	1	130–135	1.35	0.07	0.23	90	1.94	1.76
2H	3	75–80	5.90	0.33	0.51	87	1.88	1.84
3H	3	74–79	15.59	0.86	1.06	87	1.88	2.05
4H	3	62–67	25.07	1.39	1.54	90	1.94	2.34
5H	2	60–65	33.13	1.83	1.92	89	1.90	2.52
6H	2	40–42	42.51	2.35	2.31	89	1.90	2.84
7H	3	60–64	53.82	2.76	2.73	89	3.59	3.17
8H	2	95–99	62.27	3.01	3.01	90	3.64	3.59
9H	4	111–116	75.04	3.38	3.39	91	3.68	4.08
10H	4	64–69	84.17	3.65	3.64	90	3.64	4.37
11H	2	120–125	91.33	3.81	3.81	90	6.63	4.68
12H	1	134–137	99.56	3.94	4.00	89	6.56	5.01
13H	2	80–85	110.13	4.11	4.22	91	6.70	5.51
14H	2	80–82	119.71	4.27	4.41	95	7.00	6.12
15H	2	100–105	129.53	4.43	4.59	95	7.00	6.42
16H	5	90–92	143.51	4.65	4.84	95	7.00	6.61
17H	2	100–104	148.72	4.74	4.93	96	7.07	6.71
18H	2	75–79	158.07	4.89	5.08	96	7.07	6.69
19H	3	75–77	169.16	5.07	5.27	96	7.07	6.65
20H	2	75–79	177.27	5.22	5.41	96	5.47	6.46
21H	3	76–81	188.38	5.45	5.61	95	5.42	6.26
21H	5	76–78	191.37	5.51	5.66	98	5.59	6.28
22H	2	77–82	196.50	5.62	5.76	96	5.47	6.13
22H	4	78–83	199.51	5.68	5.81	96	5.47	5.95
23H	3	77–82	207.60	5.85	5.97	96	5.47	5.72
24H	3	75–79	217.17	6.05	6.16	95	5.42	5.55
24H	5	75–79	220.17	6.11	6.22	96	5.47	5.39
25H	2	75–80	225.28	6.22	6.33	97	5.53	5.39
25H	4	75–79	228.27	6.28	6.39	95	5.42	5.10
26H	2	75–79	234.87	6.42	6.54	98	5.59	5.21
26H	4	75–79	237.87	6.48	6.61	95	5.42	4.85
27H	3	85–89	246.07	6.65	6.80	96	5.47	4.71
28X	2	75–79	252.97	6.79	6.96	95	5.42	4.45
29X	4	72–79	264.36	7.03	7.25	97	5.53	4.32
30X	4	74–78	273.96	7.24	7.51	97	4.26	4.17
31X	2	72–77	280.55	7.42	7.69	98	4.31	4.06
32X	2	74–79	290.17	7.68	7.97	96	4.22	3.83
33X	2	52–54	299.53	7.94	8.25	96	4.22	3.70
34X	3	79–84	310.94	8.25	8.60	94	4.13	3.52
35X	3	70–75	320.45	8.50	8.90	94	4.13	3.42
36X	3	83–88	330.18	8.77	9.22	93	4.09	3.32
37X	3	70–75	339.65	9.03	9.53	91	4.00	3.21
38X	3	72–77	349.27	9.29	9.86	92	4.04	3.24
39X	3	72–77	358.87	9.62	10.18	94	2.79	3.25
40X	3	72–77	368.47	10.00	10.51	94	2.79	3.35
41X	3	72–77	378.07	10.37	10.83	92	2.73	3.19
42X	3	75–80	387.70	10.75	11.16	90	2.67	3.34
43X	3	83–88	397.38	11.14	11.47	93	2.76	3.43
44X	3	85–90	407.00	11.51	11.78	91	2.70	–

mbsf = meters below seafloor. The two sets of ages ($Age_{LSR, POLY}$) have been derived from our age–depth model by applying different curve fitting methods (Fig. 2). The subscripts 'LSR' and 'POLY' refer to use of the 'stepped' linear sedimentation rate model and the fourth-order polynomial equation, respectively.

Table 3
Elemental concentrations and ratios to Ti of Neogene sediment at site 590

Sample			SiO_2	Al_2O_3	Fe_2O_3T	CaO	TiO_2	LOI	Ba	Ca/Ti	Ba/Ti	Al/Ti	Si/Al
(core, section, interval(cm))			(%)	(%)	(%)	(%)	(%)	(%)	(ppm)	(g/g)	(g/g)	(g/g)	(g/g)
2H	3	75–80	5.7	1.60	0.57	49.84	0.11	41.43	154	540	0.23	13	3.15
4H	3	62–67	2.6	0.90	0.31	50.80	0.04	43.40	180	1514	0.75	20	2.55
8H	2	95–99	3.7	1.30	0.41	49.70	0.06	42.50	223	987	0.62	19	2.51
9H	4	111–116	2.9	1.00	0.44	52.04	0.07	42.68	220	886	0.52	13	2.56
12H	1	134–137	3.7	1.30	0.39	51.19	0.08	42.35	226	763	0.47	14	2.51
15H	2	100–105	1.6	0.56	0.28	52.40	0.04	43.50	132	1562	0.55	12	2.52
17H	2	100–104	1.1	0.40	0.14	52.90	0.03	43.50	94	2102	0.52	12	2.43
19H	3	75–77	1.2	0.40	0.14	54.30	0.02	43.27	142	3237	1.18	18	2.65
21H	3	76–81	0.9	0.40	0.12	53.20	0.03	43.80	124	2114	0.69	12	1.99
22H	4	78–83	1.2	0.41	0.16	53.20	0.03	43.70	99	2114	0.55	12	2.59
23H	3	77–82	1.4	0.47	0.17	52.60	0.03	43.70	191	2090	1.06	14	2.63
24H	3	75–79	1.8	0.70	0.23	54.02	0.05	43.01	165	1288	0.55	12	2.27
25H	3	72–77	1.13	0.38	0.13	52.85	0.04	44.00	161	1575	0.67	8	2.62
26H	2	75–79	1.1	0.36	0.12	52.90	0.01	43.70	139	6306	2.32	32	2.70
26H	7	20–25	1	0.36	0.09	53.24	0.02	44.00	103	3174	0.86	16	2.45
27H	3	85–89	1.3	0.44	0.24	53.00	0.03	43.40	136	2106	0.76	13	2.61
28X	2	69–75	1	0.34	0.09	53.30	0.02	44.10	119	3177	0.99	15	2.60
29X	4	72–79	0.8	0.25	0.10	53.60	0.01	43.60	114	6390	1.90	22	2.83
30X	3	72–77	1.14	0.35	0.13	52.80	0.04	44.20	91	1574	0.38	8	2.88
31X	3	73–78	1.5	0.45	0.19	53.00	0.03	43.70	156	2106	0.87	13	2.94
32X	2	74–79	1.8	0.52	0.21	52.50	0.03	43.50	160	2086	0.89	15	3.06
33X	2	52–54	1.1	0.30	0.15	53.20	0.02	43.70	173	3171	1.44	13	3.24
33X	3	20–25	2.06	0.63	0.19	52.00	0.04	43.90	184	1550	0.77	14	2.89
34X	3	84–86	1.57	0.46	0.09	52.80	0.02	44.00	218	3147	1.82	20	3.01
35X	3	70–75	2	0.59	0.19	52.50	0.02	43.30	212	3129	1.77	26	2.99
36X	1	72–77	2.35	0.71	0.19	51.80	0.04	43.80	251	1544	1.05	16	2.92
36X	3	83–88	3.6	1.00	0.31	50.70	0.04	42.50	197	1511	0.82	22	3.18
37X	3	68–70	2.81	0.73	0.30	51.10	0.06	43.60	299	1015	0.83	11	3.40
38X	3	72–77	3.2	0.90	0.73	52.46	0.06	41.69	300	1042	0.83	13	3.14
39X	3	78–80	2.36	0.72	0.27	51.70	0.05	43.70	267	1233	0.89	13	2.90
40X	3	77–79	2.76	0.88	0.39	51.70	0.04	43.40	246	1541	1.03	19	2.77
41X	3	72–77	1.8	0.60	0.25	53.96	0.03	43.16	360	2144	2.00	18	2.65

590 was deposited relatively quickly irrespective of the chosen time scale or age–depth model.

4. Samples and analytical methods

4.1. Preparation

Hole 590B was sampled at ~10 m intervals between 0 and 350 mbsf (cores 1H–44X) and at ~5 m intervals between 188 and 238 mbsf (cores 21H–26H). Individual samples are 20 cm^3 sediment 'plugs' taken according to standard Ocean Drilling Program (ODP) procedures. Based on our age–depth model (Fig. 2), these samples are typically about 270 kyr apart between 0 and 12 Ma, but about 90 kyr apart between 5.6 and 6.6 Ma.

Each sample was split in two. One half was freeze-dried, crushed to a fine powder in a porcelain mortar and pestle, and sub-sampled for whole-rock geochemical analyses. The other half was used to isolate carbonate grains including foraminifera for stable isotope analyses. Sample splits were disaggregated for 5 min in 10% hydrogen peroxide and sieved through 63, 300, 350, and 400 μm teflon meshes with distilled water. These sieved fractions were rinsed with isopropanol and left to dry in air. The fine-grained (< 63 μm) fraction was collected in a beaker and allowed

to settle for ~24 h. The beakers were then decanted and the contents were dried in an oven at 60°C for ~24 h. Six samples of the fine-grained fraction were further separated using a millipore filtration system under suction to obtain a 5–25 μm fraction. The purpose of this separation was to isolate nannofossils.

4.2. Carbonate

Carbonate concentrations were determined on 49 samples of bulk dry sediment (Table 2) using the carbonate bomb technique (Müller and Gastner, 1971). Approximately 5 ml of 10% HCl was reacted in a sealed chamber with 0.2–0.3 g of dry, powdered sediment. The volume of gas produced was measured in a graduated burette and converted to carbonate mass using a volume–mass relationship established by analyzing four standards prior to each run of 10 samples. Each sample was analyzed at least twice. Estimated errors in reported carbonate concentration are within 2% of the measured value.

4.3. Major elements and barium

Elemental concentrations were determined in the Advanced Analytical Centre, James Cook University (JCU-AAC) using X-ray fluorescence (XRF) spectrometry. Thirty-two samples of bulk dry sediment (Table 3) were fused into glass disks using a moldable crucible and analyzed for major element oxide concentrations on a Bruker-AXS SRS 3400 spectrometer. Major element concentrations (Table 3) were obtained through standard comparisons to concentration curves defined by analyses of 20 geological standards. Seven samples of the geological standard '401 MAG3' (a combination of USGS 'MAG-1' and GFS '401') were analyzed to evaluate accuracy and precision. Concentrations of all major element oxides were within 1% of the calculated regression curve and standard deviations were $<0.1\%$. The sum of all major element oxide concentrations and the loss on ignition (LOI) should be 100%. For our samples, this sum ranges between 99.6 and 100.3%. Iron contents are reported as total Fe_2O_3 (Fe_2O_3T) because Fe(II) and Fe(III) were not distinguished.

Barium concentrations were determined using a Siemens SRS-303 XRF spectrometer equipped with an LiF (110) crystal. For each sample, ~4 g of bulk sediment was made into a pressed powdered pellet and resultant Ba concentrations were determined by standard comparison to predefined concentration curves after correction for Ce interference. Multiple analyses of the MRG-1 (gabbro) and GSD-2 (stream sediment) standards averaged 63 ± 2.7 and 179 ± 8.2 ppm (1σ) compared to certified values of 61 and 185 ppm.

4.4. Stable isotopes

Stable isotope compositions of carbonate were determined in the Department of Geology and Geophysics, University of Adelaide, using a Micromass Optima mass spectrometer equipped with an automated on-line carbonate analyzer and common orthophosphoric acid bath. Several carbonate components were analyzed, including bulk sediment, bulk fine-grained material, bulk 'nannofossil' material, and extracted planktic foraminifera. In each case, approximately 200–300 μg was analyzed.

Isotopes were measured on specific-sized tests of *Orbulina universa* (>350 μm), *Globigerina bulloides* (300–350 μm), and *Globigerinoides sacculifer* (300–400 μm). These three species of planktic foraminifera were chosen to examine $\delta^{13}C$ variations between symbiotic and non-symbiotic species and between surface (<10 m) and subsurface (<300 m) waters. *Orbulina universa* hosts photosymbionts and predominantly lives in surface waters; *Gs. sacculifer* hosts photosymbionts but precipitates a final sac-like chamber at depth; *G. bulloides* does not host photosymbionts and is abundant in both surface and subsurface waters (Bé and Tolderlund, 1971; Bé, 1977; Bé et al., 1981). Size fractions were restricted to minimize $\delta^{13}C$ variations associated with test size (e.g. Ravelo and Fairbanks, 1995).

Similar morphotypes of *O. universa* and *G. bulloides* were selected. However, for *Gs. sacculifer*, two morphotypes, 'with sac' (w) and 'without sac' (w/o), were chosen. Mostly *Gs. sacculifer* w/o was extracted because this morphotype more accu-

Table 4
Carbon isotope data calculated in this study

Core-section	Interval (cm)	Depth (mbsf)	Age_{POLY} (Ma)	Bulk sediment (‰)	Bulk fine (‰)	*Gs. sacculifer* (w/o) (‰)	*Gs. sacculifer* (w) (‰)	*O. universa* (‰)	*G. bulloides* (‰)
1H-1	130–135	1.35	0.23	−0.85					−1.10
2H-3	75–80	5.90	0.51	0.56					−0.82
Replicate									−0.91
3H-3	74–79	15.59	1.06	0.72					−0.63
4H-3	62–67	25.07	1.54	0.56					−0.42
5H-2	60–65	33.13	1.92	−0.30	0.33		1.53	2.18	1.29
6H-2	40–42	42.51	2.31	−0.02	0.38	1.60		1.40	−0.63
7H-3	60–64	53.82	2.73	0.26	0.55	1.65	1.77	1.68	−0.24
8H-2	95–99	62.27	3.01	0.24	0.52			1.79	0.00
9H-4	111–116	75.04	3.39	0.72	1.13			1.80	−0.05
10H-4	64–69	84.17	3.64	0.52	0.95			1.58	−0.06
11H-2	120–125	91.33	3.81	0.75	0.85			1.55	−0.50
12H-1	134–137	99.56	4.00	0.50	0.58	1.45	1.52	1.26	0.40
Replicate				0.42			1.49		
13H-2	80–85	110.13	4.22	0.52	0.69			1.67	−0.39
14H-2	80–82	119.71	4.41	1.15	2.7	1.96	1.91	1.46	
15H-2	100–105	129.53	4.59	0.76	0.96			1.56	−0.25
16H-5	90–92	143.51	4.84	1.02	1.23			1.59	0.27
17H-2	100–104	148.72	4.93	1.13	1.38			1.70	0.30
18H-2	75–79	158.07	5.08	1.13	1.51	1.68		1.65	
19H-3	75–77	169.16	5.27	1.38	1.61	1.79	1.94	2.19	0.49
Replicate				1.38					
20H-2	75–79	177.27	5.41	1.40	1.63	1.92		1.86	
21H-3	76–81	188.38	5.61	1.66	1.78		1.88	1.93	−0.29
21H-5	76–78	191.37	5.66	1.33	1.5	1.86		1.56	
22H-2	77–82	196.50	5.76	0.94	1.091	1.79			0.19
Replicate				0.94					
22H-4	78–83	199.51	5.81	1.22	1.2	1.71		1.19	−0.02
23H-3	77–82	207.60	5.97	1.45	1.52	1.83		1.48	0.17
24H-3	75–79	217.17	6.16	1.24	1.31	1.73		1.91	0.08
24H-5	75–79	220.17	6.22	1.58	1.38			2.36	
25H-2	75–80	225.28	6.33	1.43	1.44	2.00		1.57	
25H-4	75–79	228.27	6.39	0.97	1.09	1.96		1.11	−0.88
26H-2	75–79	234.87	6.54	1.25	1.19	1.99		1.36	−0.41
26H-4	75–79	237.87	6.61	1.09	1.16	1.55		1.50	
27H-3	85–89	246.07	6.80	1.13	1.28	1.56		1.55	
28X-2	75–79	252.97	6.96	1.42	1.53	2.05	2.03	1.56	
29X-4	72–79	264.36	7.25	1.50	1.65	2.53			
30X-4	74–78	273.96	7.51	1.10	1.35	1.97		1.82	
31X-2	72–77	280.55	7.69	1.33	1.5			1.92	
32X-2	74–79	290.17	7.97	1.36	1.46	2.38		2.40	
33X-2	52–54	299.53	8.25	1.27	1.43	2.39		2.14	
34X-3	79–84	310.94	8.60	0.90					
35X-3	70–75	320.45	8.90	1.26					
36X-3	83–88	330.18	9.22	1.21					
37X-3	70–75	339.65	9.53	0.76					
38X-3	72–77	349.27	9.86	0.56					
39X-3	72–77	358.87	10.18	0.48					
40X-3	72–77	368.47	10.51	0.98					
41X-3	72–77	378.07	10.83	1.22					
42X-3	75–80	387.70	11.16	1.33					
43X-3	83–88	397.38	11.47	0.93					
44X-3	85–90	407.00	11.78	1.14					

Gs. Sacculifer (w/o) and (w) refer to 'without sac' and 'with sac', respectively.

rately records surface water $\delta^{13}C$ (Spero and Lea, 1993).

Sixteen samples of the NBS19 limestone standard were analyzed with other samples to evaluate the accuracy and precision of $\delta^{13}C$ measurements. The mean of these analyses was 1.95‰ ± 0.05‰ (1σ) compared to the consensus value of 1.95‰ (Coplen et al., 1983). Five samples from site 590 (Table 4) were also analyzed twice. These replicate analyses were all within 0.1‰.

4.5. Scanning electron microscopy

Bulk sediment samples from cores 6H and 30X were examined for primary components. Approximately 0.2 g of wet bulk sediment was placed on a 1 cm diameter stub, coated with gold, and analyzed using a Philips scanning electron microscope (SEM) at the JCU-AAC.

5. Results

5.1. Bulk sediment composition

Biogenic $CaCO_3$ dominates upper Neogene sediment at site 590. Carbonate concentrations vary from 87 to 98% for bulk sediment (Table 2; Fig. 3), in agreement with previous work (Stein and Robert, 1986). Moreover, upper Neogene sediment has CaO between 49.7 and 54.3%, and LOI between 41.4 and 44.2% (Table 3). Because pure calcite renders CaO and LOI concentrations of 56 and 44%, respectively, our XRF results also suggest between 91.3 and 97.6% $CaCO_3$. Most of this $CaCO_3$ is comprised of coccoliths between 3 and 10 μm in diameter (Fig. 4), although foraminifera tests are common.

The non-carbonate fraction at site 590 consists mostly of aluminosilicate clays. After CaO, the most abundant metal oxides are SiO_2 and Al_2O_3 (Table 3). However, concentrations of both oxides are relatively low (< 5.7 and < 1.6%, respectively) and generally covary ($r^2 = 0.95$) with each other (Fig. 3). The Si/Al ratio in our samples is ~2.7 g/g (Table 3), which is typical of smectite clays (e.g. Faure, 1998). Indeed, smectites dominate (40–100%) the non-carbonate fraction of sediment from the Lord Howe Rise (Stein and Robert, 1986). Biogenic Si tests are conspicuously absent.

5.2. Carbonate accumulation

Carbonate mass accumulation rates (MARs) provide one record of export production at site 590 because coccoliths dominate bulk carbonate. These MARs were calculated (g/(cm^2 kyr)) for each sample according to:

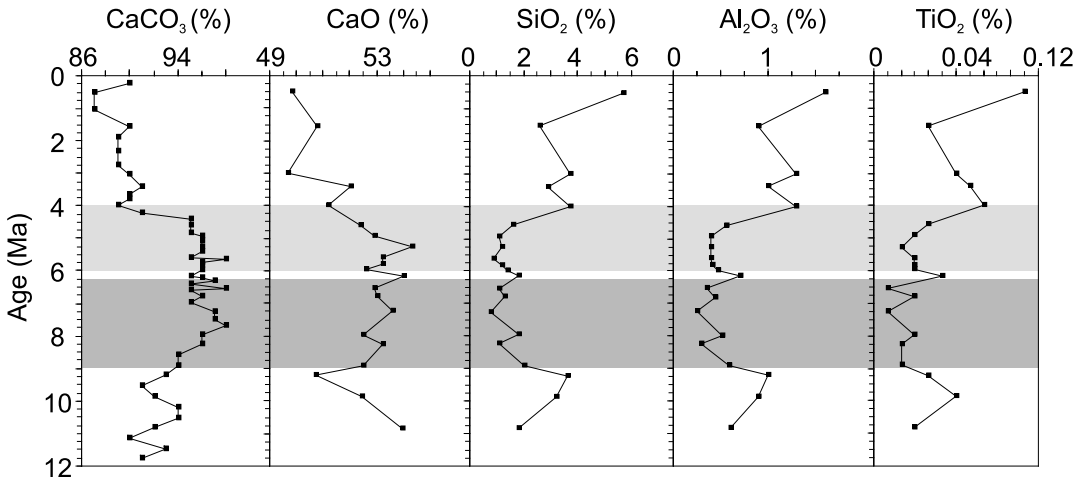

Fig. 3. Carbonate and elemental oxide concentrations at site 590. Sample ages are from 'Age$_{POLY}$', Table 2. The two shaded areas indicate time intervals of inferred elevated productivity based on different proxies (see Section 6.1).

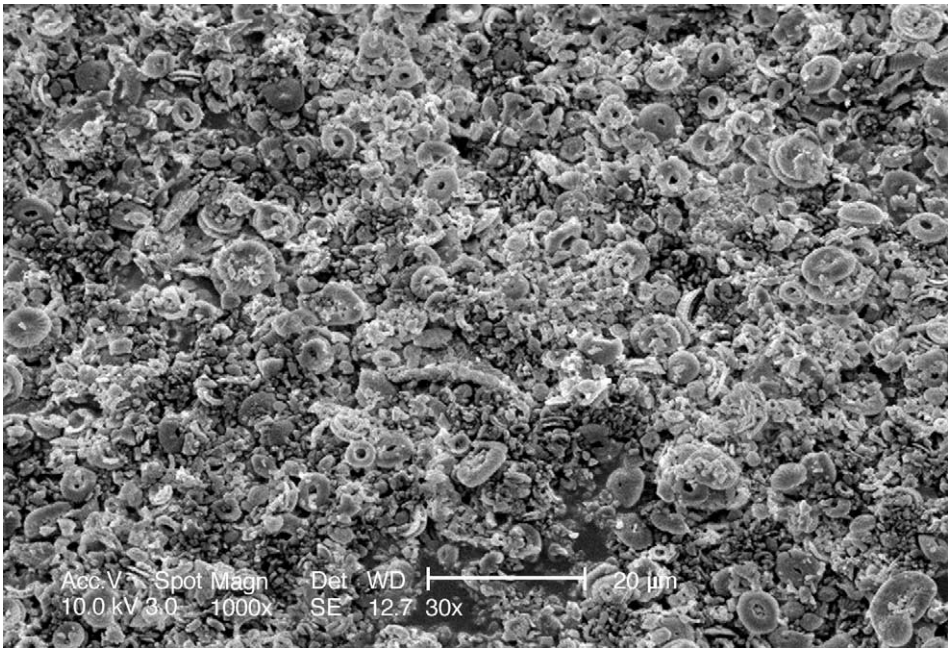

Fig. 4. Scanning electron microscope (SEM) photograph of bulk sediment from sample 590B-30X4, 74–78 cm. Note that the sediment is almost entirely composed of coccoliths.

$$CaCO_3\ MAR = wt\%\ CaCO_3 \times SR \times DBD \quad (1)$$

where SR is the sedimentation rate (cm/kyr) taken from age–depth models (Fig. 2) and DBD is the dry bulk density (g/cm^3). The DBD was estimated from:

$$DBD = (1-\phi/100) \times \rho \quad (2)$$

where ϕ is the wet porosity of sediment and ρ is the density of sediment particles (Table 2). Porosity data for our samples were extrapolated from the nearest sample analyzed for physical properties (Morin, 1986). The particle density is approximately 2.7 g/cm^3, given that the sediment is almost entirely carbonate.

Both the stepped and polynomial SR curves were used to calculate $CaCO_3$ MARs (Fig. 5). With the stepped LSR curve, $CaCO_3$ MARs vary between 3 and 4 g/(cm^2 kyr) older than 9 Ma, 4 and 4.6 g/(cm^2 kyr) between 9 and $\sim$7 Ma, and $>$5 g/(cm^2 kyr) from $\sim$7 to 3.8 Ma. MARs are highest ($\sim$7 g/(cm^2 kyr)) between 5 and 4.3 Ma. Younger than 3.8 Ma, MARs are generally $<$3 g/(cm^2 kyr). The polynomial SR curve gives a similar, though smoothed, trend. In this case, $CaCO_3$ MARs average $\sim$3.6 g/(cm^2 kyr) between 12 and 9 Ma, gradually increase to a maximum of 6.7 g/(cm^2 kyr) at 4.9 Ma, and gradually decrease to a minimum of 1.5 g/(cm^2 kyr) at 0.2 Ma. Carbonate MARs were anomalously high at site 590 in the earliest Pliocene.

As stressed by several authors (e.g. Dickens and Owen, 1994; Farrell et al., 1995; Filippelli and Delaney, 1995; Murray et al., 1995), calculated MARs effectively mimic the SR curve in uniform sediment sections with similar physical properties, such as site 590. Incorrect SR curves (e.g. through poorly placed age datums) will therefore lead to inaccurate MARs. This potential problem can be evaluated by normalizing the component of interest to one with a different sedimentary behavior (e.g. Murray et al., 1993; Dickens and Owen, 1994). In the case of $CaCO_3$ or other biological proxies, Ti is an ideal normalizing element because, in many open-ocean environments, Ti is dominantly hosted in aluminosilicate phases,

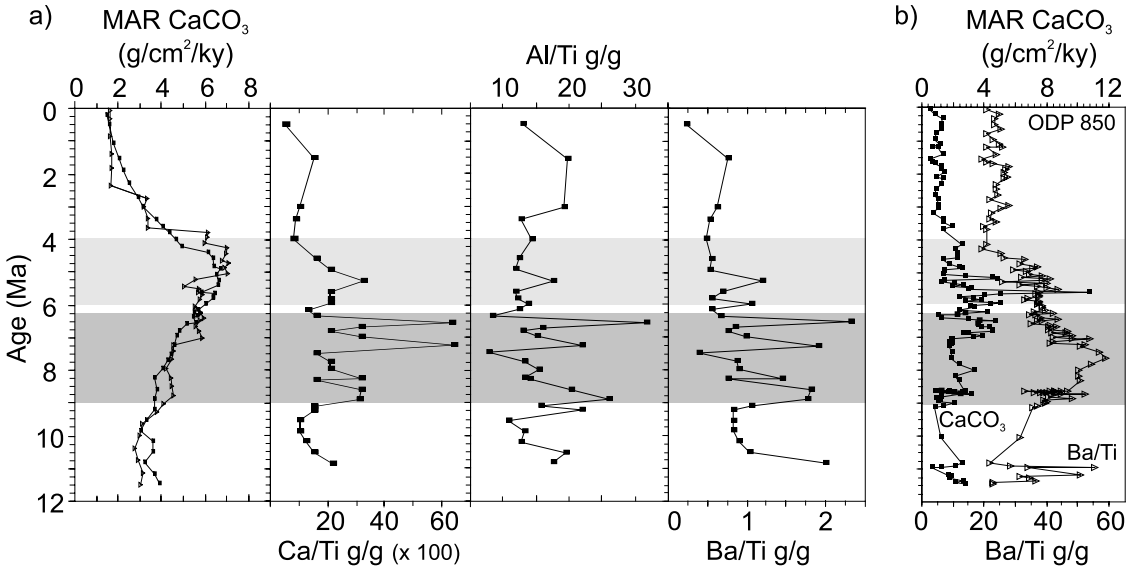

Fig. 5. (a) Carbonate MARs and Ca/Ti, Ba/Ti, Al/Ti ratios at site 590. The carbonate MARs have been calculated using LSRs (△) and smoothed SRs (■). (b) Carbonate MARs (■) and Ba/Ti ratios (△) at ODP site 850 (Schroeder et al., 1997). Data have been calibrated to the time scale of Berggren et al. (1995a,b) to permit comparison with site 590 data.

added through aeolian processes, and generally immobile after deposition (Goldberg and Arrhenius, 1958; Murray et al., 1993; Murray and Leinen, 1996). At site 590, Ca/Ti ratios are <2200 g/g between 10.8 and 9 Ma, increase to >3200 g/g by 8.3 Ma, and then oscillate between 6600 and 2000 g/g until 6.2 Ma. A peak in Ca/Ti of 3350 g/g, occurring between 6.2 and 5.3 Ma, is followed by an overall decline until 0.5 Ma. Both the $CaCO_3$ MARs and Ca/Ti ratios are elevated in the latest Miocene, although peak $CaCO_3$ MARs occur in the earliest Pliocene when Ca/Ti ratios are relatively low (Fig. 5).

5.3. Barium and aluminum deposition

Barium and Al records probably also track past changes in export production at site 590. Marine barite ($BaSO_4$) forms in microenvironments when organic matter decomposes in the water column following uptake of dissolved Ba^{2+} (Dehairs et al., 1980; Bishop, 1988). As a consequence, Ba fluxes to the seafloor can relate to surface productivity, especially in pelagic sediments dominated by biogenic components (e.g. Goldberg and Arrhenius, 1958; Chow and Goldberg, 1960; Dymond, 1981; Dymond et al., 1992; Dickens and Owen, 1996; Schroeder et al., 1997). Dissolved Al^{3+} is scavenged from seawater by biogenic particles (Orians and Bruland, 1986; Moran and Moore, 1988a,b; Murray et al., 1993). Although aluminosilicate accumulation dominates the total Al flux to the seafloor in many environments, the scavenged component may comprise a significant portion in locations with low total Al (Murray et al., 1993; Murray and Leinen, 1996).

The accumulation of Ba and Al with respect to Ti generally declines from the late Miocene to the Pleistocene (Fig. 5). The Ba/Ti ratio varies between 0.5 and 1.4 g/g from 10.8 to 6.5 Ma, peaking at 6.5 Ma. Afterwards, Ba/Ti ratios are <0.7 g/g, decreasing to 0.2 g/g at 0.5 Ma. The Al/Ti ratio varies between 15 and 36 g/g from 10.8 to 6.5 Ma, and then drops to between 13 and 23 g/g from 6.5 to 0.5 Ma. Downcore trends in both records covary to a certain extent ($r^2=0.54$) with changes in the Ca/Ti record (Fig. 5).

5.4. Stable carbon isotopes

All $\delta^{13}C$ records of carbonate at site 590 display a significant decrease in upper Miocene–lower

Table 5
Comparison of $\delta^{13}C$ results for the bulk sediment fractions

Sample (Core, section, interval (cm))			Bulk sediment (‰)	Bulk fine (< 63 μm) (‰)	Bulk nannofossils (5–25 μm) (‰)	$\delta^{13}C$ range (‰)
7H	3	60–64	0.26	0.55	0.47	0.29
13H	2	80–85	0.52	0.69	0.61	0.17
19H	3	75–77	1.38	1.61	1.45	0.23
24H	3	75–79	1.24	1.31	1.23	0.08
27H	3	85–89	1.13	1.28	1.16	0.15
33X	2	52–54	1.27	1.43	1.38	0.16

The $\delta^{13}C$ range has been calculated as the difference between the maximum and minimum $\delta^{13}C$ values for each sample.

Pliocene sediment. However, the magnitude and timing of this shift depends on the phase analyzed.

Bulk sediment $\delta^{13}C$ ranges between −0.85 and +1.66‰, with an overall decline over the past 12 Myr (Table 5; Fig. 6). Except for low values (~0.5‰) between 10.2 and 9.5 Ma, $\delta^{13}C$ is relatively high (>0.9‰) until about 5 Ma, reaching a maximum of 1.66‰ at 5.6 Ma. The minimum $\delta^{13}C$ of bulk sediment occurs at 0.2 Ma after a minor high between 1.5 and 0.5 Ma. Most of the decline in bulk sediment $\delta^{13}C$ (−1.96‰) thus occurs between 5.6 and 1.9 Ma. Although the $\delta^{13}C$ of fine-grained and 'nannofossil' material usually exceeds that of bulk sediment, $\delta^{13}C$ varies <0.29‰ in any sample analyzed for all three components (Table 4). Thus, as might be expected for coccolith-rich sediment, the $\delta^{13}C$ of bulk sediment at site 590 effectively records the $\delta^{13}C$ of $CaCO_3$ tests from surface waters.

Similar to bulk sediment, the $\delta^{13}C$ of surface-dwelling planktic foraminifera decreases over the last 12 Myr. Previous stable isotope work at site 590 (Elmstrom and Kennett, 1986) investigated the $\delta^{13}C$ of *Globigerinoides sacculifer* but did not distinguish between morphotypes. Our $\delta^{13}C$ re-

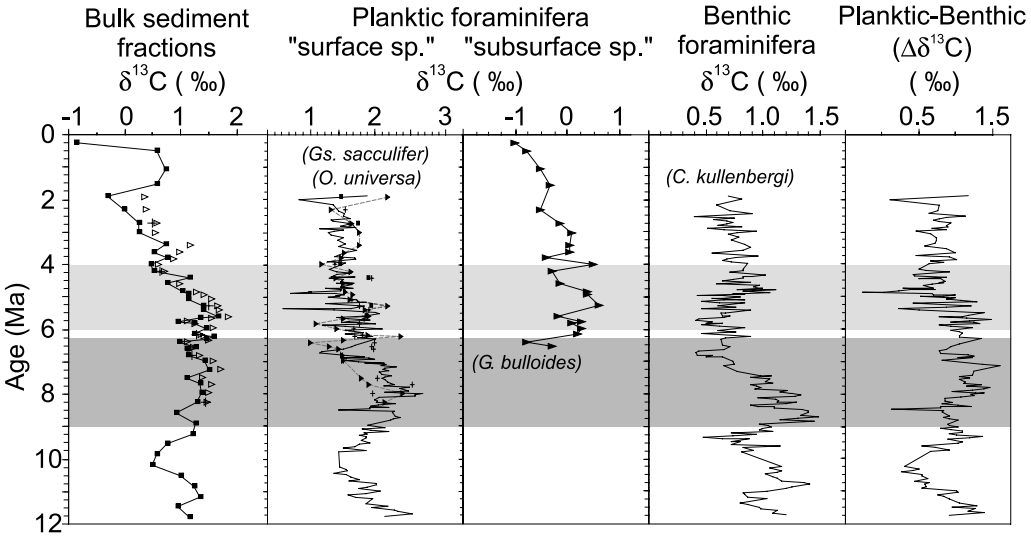

Fig. 6. The $\delta^{13}C$ of bulk sediment fractions, planktic foraminifera, and benthic foraminifera from site 590. Bulk sediment fractions include bulk sediment (■), bulk fine-grained sediment (△), and bulk 'nannofossils' (+). Planktic foraminifera have been grouped into surface-dwelling species [*Gs. sacculifer* 'w' (■), *Gs. sacculifer* 'w/o' (+), *Gs. sacculifer* 'mix' (−), *O. universa* (-▲-)] and subsurface-dwelling species [*G. bulloides*], where *Gs. sacculifer* 'mix' is the mixed-morphotype data from Elmstrom and Kennett (1986). The $\Delta\delta^{13}C$ record has been calculated from *Gs. sacculifer* 'mix' and *Cibicidoides kullenbergi* using data from Elmstrom and Kennett (1986). Foraminiferan $\delta^{13}C$ values have not been corrected for vital effects.

cords of *Gs. sacculifer* (w) and (w/o) are similar to each other. Moreover, there is no significant difference between the $\delta^{13}C$ records of *Gs. sacculifer* (w, w/o, and mix) and *Orbulina universa*. We therefore discuss all surface-dwelling planktic foraminifera records together (Fig. 6).

The $\delta^{13}C$ of *Gs. sacculifer* and *O. universa* ranges between 0.72 and 2.67‰, a range slightly less and about 1‰ heavier than for bulk sediment $\delta^{13}C$. Between 11.8 and 8.3 Ma, $\delta^{13}C$ decreases temporarily. At about 8 Ma the record peaks; $\delta^{13}C$ values then fall by nearly 1‰ over 0.5–1.5 Myr, depending on which record is examined (Fig. 6). Thus, the timing of the pronounced shift in the $\delta^{13}C$ of surface-dwelling planktic foraminifera occurs between 7.8 and 6.4 Ma at site 590, or 0.8 Myr before that in bulk sediment. The $\delta^{13}C$ record subsequently shows high-amplitude (1.64‰) fluctuations between 6.3 and 5.0 Ma, and relatively constant, lower values afterwards.

The $\delta^{13}C$ record of *Globigerina bulloides* (Fig. 6) only begins at 6.5 Ma. Its range (−1.10 to 0.49‰) is lower than that of bulk carbonate and surface-dwelling planktic foraminifera, as expected for a planktic species commonly found in subsurface water. However, the overall trend of this $\delta^{13}C$ record is different from that of surface-dwelling planktic foraminifera but somewhat similar to that of bulk carbonate.

A benthic foraminifera $\delta^{13}C$ record has been constructed at site 590 using tests of *Cibicidoides kullenbergi* (Elmstrom and Kennett, 1986) (Fig. 6). This record has been discussed previously (Elmstrom and Kennett, 1986; Kennett, 1986), although with a different time scale (Berggren et al., 1985). Using a revised time scale, the $\delta^{13}C$ drops temporarily between 10.8 and 9.3 Ma, reaches a maximum at 8.7 Ma, then declines towards 6.7 Ma. Despite a slight increase ca. 5 Ma, $\delta^{13}C$ values remain relatively low for the remainder of the record.

6. Discussion

6.1. The timing of enhanced productivity

Bulk sediment carbonate MARs, Ba/Ti ratios, and Al/Ti ratios at site 590 were two to three times higher during the latest Miocene and earliest Pliocene relative to previous and subsequent time intervals (Fig. 5). Similar observations have been made at other sites beneath upwelling regions of the Indian and Pacific oceans (e.g. Van Andel et al., 1975; Kennett et al., 1986; Peterson et al., 1992; Berger et al., 1993; Farrell et al., 1995; Dickens and Owen, 1999). Records of $CaCO_3$, Ba, opal, and organic carbon accumulation at ODP site 850 in the eastern Equatorial Pacific (Schroeder et al., 1997) are especially pertinent for comparison. Between 9.0 and 4.0 Ma, on the Berggren et al. (1995a,b) time scale, all of these records show extremely variable accumulation, with rates typically two to three times higher than during previous and subsequent time intervals. Following other work (e.g. Farrell et al., 1995; Filippelli and Delaney, 1995), Schroeder et al. (1997) linked these elevated late Miocene–early Pliocene biogenic accumulation rates to elevated productivity in the overlying equatorial Pacific surface waters and the 'biogenic bloom' phenomenon. The same general explanation is offered for changes in sediment composition at site 590. Our records indicate that the biogenic bloom occurred at the TF between ca. 9 and 3.8 Ma. This is broadly coincident with the timing of enhanced productivity at other upwelling regions in the Indian and Pacific oceans (Dickens and Owen, 1999).

There is a distinct offset between the timing of maximum $CaCO_3$ MARs and maximum Ca/Ti, Ba/Ti and Al/Ti ratios at site 590. Carbonate MARs are highest between 6 and 4 Ma, whereas the elemental ratios are highest between 9.0 and 6.5 Ma. A similar temporal offset has been documented (although not explained) at ODP site 850, where $CaCO_3$ and Ba MARs are highest between 7 and 5 Ma but Ba/Ti ratios are highest between 9 and 7 Ma (Schroeder et al., 1997) (Fig. 5). Temporal offsets between productivity proxies during the biogenic bloom interval have been discussed in the literature (Dickens and Owen, 1999). However, these discrepancies were between paleoproductivity records from different sites and could be explained by lateral movements of elevated surface productivity regions over time (Dickens and

Owen, 1999). Disparities between $CaCO_3$ MARs and elemental ratios at the same location must have a different explanation, such as misplaced age datums, variable elemental fluxes, carbonate dissolution, or a change in the carbonate flux relative to the organic carbon flux. The two latter explanations can be excluded because $CaCO_3$ MAR and Ca/Ti variations are temporally offset (Fig. 5). Either the age model is wrong or the Ti flux changed over time.

Misplaced depths of biostratigraphic datums would lead to erroneous SRs and incorrect MARs. The key datums used to determine SRs in upper Miocene and lower Pliocene sediment at site 590 are the FAD *Amaurolithus primus*, FAD *Ceratolithus rugosus*, and LAD *Reticulofenestra pseudoumbilicus* (Table 1; Fig. 2). Given that these datums were identified in samples spaced ~10 m apart (Kennett et al., 1986), depths of LADs and FADs could be 10 m too high and 10 m too low, respectively. Taking these potential errors into account, SRs could be up to 1.5 cm/kyr higher between 5.1 and 3.8 Ma but remain essentially the same between 7.2 and 5.1 Ma (Fig. 7). A realignment of datums cannot explain the significant time offset between $CaCO_3$ MARs and key elemental ratios.

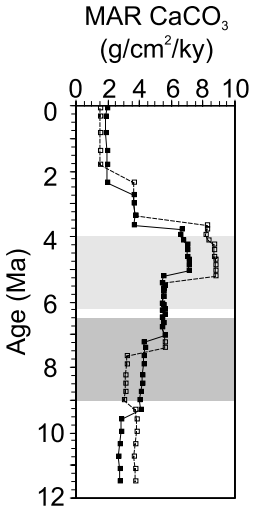

Fig. 7. Possible deviations in the calculation of carbonate MARs as a function of varying the LSRs at site 590. Carbonate MARs have been calculated using LSRs derived from depth-averaged datums (■), and from the minimum (LAD) or maximum (FAD) depth in a sampling interval (□).

Changes in the Ti flux can influence Ca/Ti, Ba/Ti, and Al/Ti ratios of bulk sediment. In particular, increases in either the flux or Ti content of terrigenous material would cause all three ratios to decrease, although by different amounts because common aluminosilicate minerals contain relatively little Ca and Ba. After 6.5 Ma, Al/Ti decreases by a factor of 2.5 whilst Ca/Ti and Ba/Ti decrease by a factor of at least four. Moreover, much of the change stems from fluctuations in Ti and Al contents rather than fluctuations in Ca and Ba contents (Table 3). Bulk chemistry changes are consistent with a greater input or higher Ti content of terrigenous material since the Pliocene. Stein and Robert (1986) estimated past terrigenous fluxes at site 590 from MARs of carbonate-free sediment (MARTs) and smectite/illite ratios. In the early Pliocene, MARTs increased from less than 0.5 to greater than 1.0 g/(cm^2 kyr). A sharp decline in smectite/illite ratios during this time may indicate intensified wind strength and aeolian transport of illite (Stein and Robert, 1986). Increased delivery of Ti after 6.5 Ma best explains the relatively low Ca/Ti, Ba/Ti, and Al/Ti ratios during a time of high $CaCO_3$ MARs.

6.2. Carbon isotopes

Consistent with the sediment chemistry records, certain $\delta^{13}C$ records from site 590 suggest increased productivity during the latest Miocene and earliest Pliocene. The bulk sediment $\delta^{13}C$ record reaches its highest values between 9 and 5 Ma (Fig. 6). This signal probably reflects variations in surface water $\delta^{13}C$ because coccoliths dominate the bulk sediment (Fig. 4). A straightforward interpretation of this signal is that enhanced productivity removed greater amounts of ^{12}C from surface waters. Such a change in carbon cycling should also affect the gradient between surface and intermediate water $\delta^{13}C$. We have calculated this gradient over time at site 590 by comparing coeval planktic and benthic foraminiferan $\delta^{13}C$ records (Elmstrom and Kennett, 1986). The $\Delta\delta^{13}C$ (planktic–benthic) record ranges between −0.27

and 1.60‰ but is generally highest between 8.4 and 5.3 Ma (Fig. 6). The steepened gradient in the latest Miocene and earliest Pliocene supports enhanced productivity during this time.

However, distinct temporal offsets between the different $\delta^{13}C$ records significantly complicate relationships between carbon isotopes and productivity at site 590. In particular, a decrease of ~1‰ in the $\delta^{13}C$ of surface-dwelling planktic foraminifera occurs ~2 My before a similar decrease in bulk carbonate (Fig. 6). A similar offset exists at ODP site 704 in the Southern Ocean (Mead et al., 1991), the only other site with comparable bulk carbonate and foraminiferal $\delta^{13}C$ records. We offer two general explanations for the discrepancy between nannofossil and planktic foraminifera $\delta^{13}C$ records at site 590.

First, either the $\delta^{13}C$ record of bulk sediment or surface-dwelling planktic foraminifera includes carbonate precipitated out of isotopic equilibrium with ambient seawater. Environmental parameters (e.g. alkalinity, temperature, irradiance) and physiological processes, or 'vital effects', can shift the $\delta^{18}O$ and $\delta^{13}C$ of coccoliths and planktic foraminifera from +1‰ to −2.5‰ relative to expected equilibrium values (e.g. Anderson and Cole, 1975; Vergnaud-Grazzini, 1976; Kahn, 1979; Dudley et al., 1980; Goodney et al., 1980; Dudley and Nelson, 1994; Spero et al., 1997; Bemis et al., 2000). Despite these effects on isotope fractionation, several coccolithophore species and *Orbulina universa* accurately track changes in seawater $\delta^{13}C$ over time (Dudley et al., 1986; Williams et al., 1977; Spero, 1992), suggesting that disequilibrium fractionation, if any, remains relatively constant for individual species. A change in environmental conditions or in the relative abundances of coccolithophorid species with different vital effects could cause discrepancies between $\delta^{13}C$ records of bulk nannofossils and surface-dwelling planktic foraminifera (Paull and Thierstein, 1987; Dudley and Nelson, 1994). The first possibility does not adequately explain why different species of benthic and planktic foraminifera record roughly coincident negative shifts in $\delta^{13}C$ ca. 7 Ma. The second possibility is plausible because the coccolith assemblage at site 590 changes in the early Pliocene (Fig. 8; Lohman, 1986), coincident with the marked negative excursion in bulk sediment $\delta^{13}C$ (Fig. 6).

An alternative and more straightforward explanation for differences in 'mixed layer' $\delta^{13}C$ rec-

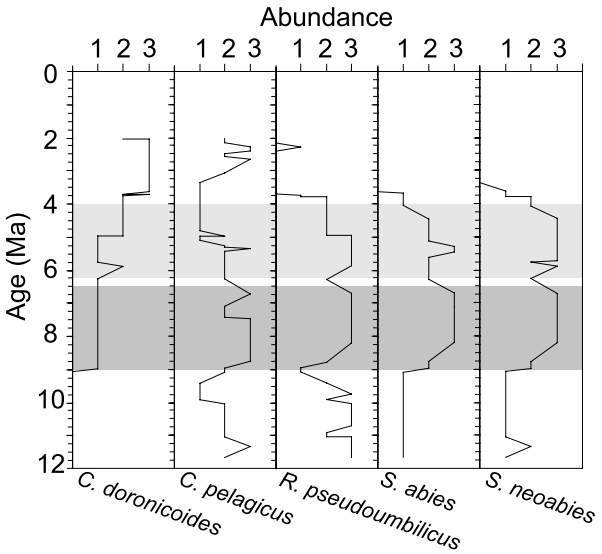

Fig. 8. Variations in nannofossil abundance over time at site 590 (from Lohman, 1986) for the five most abundant species at this site (*Crenalithus doronicoides*, *Coccolithus pelagicus*, *Reticulofenestra pseudoumbilicus*, *Sphenolithus abies*, and *Sphenolithus neoabies*). The *x*-axis is graded between 'rare' (1), 'common' (2), and 'abundant' (3).

ords is that nannofossils and surface-dwelling planktic foraminifera precipitate their tests at different water depths. In upwelling areas, most coccolithophores occur at the sea surface (Hagino et al., 2000). The $\delta^{13}C$ of coccoliths should therefore relate to surface water $\delta^{13}C$ (Anderson and Steinmetz, 1981; Dudley and Nelson, 1989). On the other hand, although certain planktic foraminifera are often classified as 'surface dwellers', these species are not precluded from deeper habitats (Bé and Tolderlund, 1971; Bé, 1977). We have analyzed *Gs. sacculifer* (w) and (w/o) in the same sample and find minimal offset (<0.15‰) between the two morphotypes. This may indicate a similar $\delta^{13}C$ composition of seawater over the depth at which the morphotypes precipitated their tests. Given the coherent $\delta^{13}C$ records of *O. universa* and *Globigerinoides sacculifer*, it is possible that the tests of these species have precipitated $\delta^{13}C$ over a larger depth range than the coccoliths. Indeed, Kahn and Williams (1981) suggested that precipitation of foraminifera tests is not restricted to the depth interval where the highest total standing crop occurs. In this case, temporal offsets between different $\delta^{13}C$ records might be viewed as a series of changes in the carbon isotope gradient of the water column.

6.3. Paleoceanography at the Tasman Front

The $\delta^{13}C$ records of bulk carbonate and foraminifera at site 590 probably track changes in $\delta^{13}C$ at different water depths. These depths would include: the surface, a shallow mixed layer (nominally ≤ 10 m), and deep intermediate water (nominally ≤ 1300 m). By combining these changes in $\delta^{13}C$ with sediment proxies for productivity, we can develop a coherent picture for paleoceanographic changes at the TF (Fig. 9).

Between 9.5 and 8 Ma, $CaCO_3$ MARs rose, minor peaks in Ba/Ti and Al/Ti ratios occurred, and the $\delta^{13}C$ of bulk carbonate and planktic foraminifera increased slightly (Figs. 5, 6). All of these observations support escalating primary production and excess removal of ^{12}C from surface waters. From 8.0 to 6.5 Ma, $CaCO_3$ MARs rose, the Ca/Ti, Ba/Ti, and Al/Ti ratios reached maximum values, and the $\delta^{13}C$ of planktic and benthic foraminifera dropped significantly (Figs. 5 and 6). The $\delta^{13}C$ of 'subsurface' planktic foraminifera is also relatively low. The steep $\delta^{13}C$ gradient during this time compares to that in modern frontal regions with significant upwelling and elevated surface productivity (Kroopnick, 1985). The overall depletion in the $\delta^{13}C$ profiles may indicate

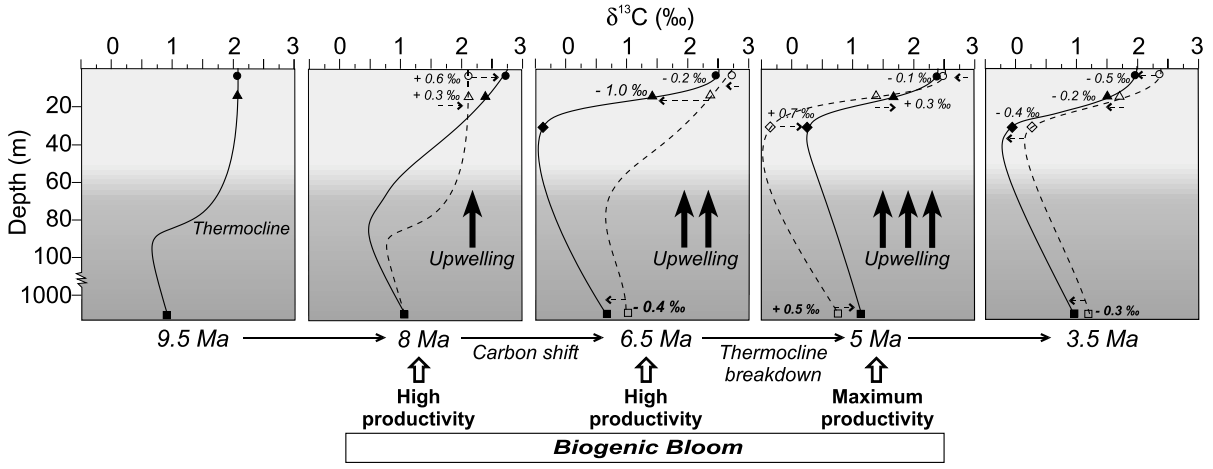

Fig. 9. Carbon isotope vertical profiles at site 590 represented schematically based on the $\delta^{13}C$ records of bulk carbonate (●), *Gs. sacculifer* 'mix' (▲), *G. bulloides* (♦) and *C. kullenbergi* (■) for the late Miocene and early Pliocene. Bulk carbonate $\delta^{13}C$ values have been corrected by +1‰, given the assumption that the $\delta^{13}C$ gradient through the mixed layer was minimal prior to the start of the biogenic bloom and the Chron C3AR carbon shift. Recorded $\delta^{13}C$ shifts are quantified (e.g. +1‰ →) so that the change in the $\delta^{13}C$ gradient between successive 1.5 Myr intervals (dashed line) can be inferred.

a global decrease in the $\delta^{13}C$ of seawater. However, if this is the case, coccolithophorids must have been isolated from the rest of the water column by a shallow thermocline (or another kind of pycnocline) because there is only a very slight decrease in bulk carbonate $\delta^{13}C$. Collectively, all lines of evidence suggest increased upwelling and primary production at the TF, a view entirely consistent with changes in microfossil assemblages (Elmstrom and Kennett, 1986). Between 6.5 and 5 Ma, the $\delta^{13}C$ of bulk carbonate decreased very slightly while that of planktic (surface and subsurface) and benthic foraminifera increased. As a result, the $\delta^{13}C$ gradient weakened, implying a decrease in primary productivity or a loss in the density stratification of the water column. Given that this period coincides with maximum $CaCO_3$ MARs and apparently increased fluxes of windblown material, upwelling at the TF may have intensified. This scenario again agrees with microfossil studies at site 590 (Elmstrom and Kennett, 1986; Kennett and von der Borch, 1986). Between 5 and 3.5 Ma, all $\delta^{13}C$ records decreased, although by varying amounts, suggesting a decrease in the $\delta^{13}C$ of seawater and in the $\delta^{13}C$ gradient of the water column. At site 590, the latter is probably linked to reduced primary production, given that $CaCO_3$ MARs decline over the same period.

6.4. Global nutrient and carbon cycling in the late Neogene

Various sedimentary records indicate that surface water productivity and burial of key nutrients (e.g. P, SiO_2) increased at upwelling zones of the Indian and Pacific oceans between ca. 9.0 and 3.5 Ma (Dickens and Owen, 1999). Because primary productivity is limited by the availability of nutrients with short (<100 kyr) residence times, this observation – the biogenic bloom – implies (e.g. Farrell et al., 1995; Dickens and Owen, 1999; Hermoyian and Owen, 2001): (1) an elevated supply of nutrients to the oceans, (2) a redistribution of nutrients within the global ocean, or (3) both.

Two recent papers (Filippelli, 1997; Hermoyian and Owen, 2001) have emphasized that the biogenic bloom signifies an increase in nutrient delivery to the oceans. Although mountain uplift and weathering probably increased during the latest Miocene and earliest Pliocene (e.g. Raymo et al., 1988; Dobson et al., 2001), this explanation ignores compelling evidence for profound changes in global oceanography that would have redistributed nutrients between 8 and 4 Ma. For example, the maximum depth of the carbonate compensation depth (CCD) switched from the Atlantic to the Pacific, suggesting a shift in deep water flow (e.g. Van Andel, 1975; Rea and Leinen, 1985); the West Antarctic ice sheet developed, leading to large-scale production of Antarctic Bottom Water (e.g. Drewry, 1978; Ciesielski et al., 1982); and the Isthmus of Panama emerged, separating Pacific and Atlantic circulation (e.g. Keigwin, 1982; Farrell et al., 1995; Haug and Tiedemann, 1998).

Our work at site 590 also challenges two key arguments used as support for increased global burial of nutrients. First, Filippelli (1997) has interpreted the high in bulk carbonate $\delta^{13}C$ during the latest Miocene and earliest Pliocene (e.g. Fig. 6) as representing greater burial of organic matter in the oceans. However, this argument neglects the fact that $\delta^{13}C$ values of both planktic and benthic foraminifera decrease during this same interval at site 590 (Fig. 6) and elsewhere (e.g. Vincent et al., 1980, 1985; Berger and Vincent, 1986). Clearly, the entire oceanic carbon pool did not become enriched in ^{13}C as expected by a straightforward increase in the output of organic carbon. We strongly suggest instead that $\delta^{13}C$ records of different phases diverge during the biogenic bloom because water mass structures have changed (Fig. 9). Second, Hermoyian and Owen (2001) have calculated late Neogene phosphorus MARs at sites beneath the central Indian Ocean gyre, suggesting that these rates increase during the biogenic bloom. This observation, if correct, provides an interesting argument for a truly global rise in nutrient burial. However, as highlighted in our paper (Figs. 2 and 5) and elsewhere (e.g. Dickens and Owen, 1994), the integrity of MAR records depends strongly upon excellent stratigraphy. Unlike at site 590, the sites chosen beneath the central Indian Ocean gyre

have very poor stratigraphic control (Dickens and Owen, 1999).

At present, site 590 is the only location where multiple elemental and isotopic proxies for past productivity have been measured across the biogenic bloom interval. The suite of records at site 590 indicates that distinct shifts in the $\delta^{13}C$ of seawater accompanied the biogenic bloom phenomenon, supporting previous suggestions that the Chron C3AR carbon shift was at least partly associated with elevated primary production (Vincent et al., 1980, 1985). Moreover, at this location, the biogenic bloom can be separated into two components: an early phase characterized by maximum accumulation of Ba, Al, and Ca relative to Ti and a depletion in foraminiferan $\delta^{13}C$ (the Chron C3AR carbon shift); and a late phase characterized by maximum $CaCO_3$ MARs and a depletion in nannofossil $\delta^{13}C$.

7. Conclusions

Site 590, beneath the modern TF in the Tasman Sea, contains a thick section of predominantly biogenic carbonate. Sediment deposited between ca. 9 and 3.8 Ma shows abundant evidence for elevated primary productivity, including a two- to three-fold escalation in carbonate MARs, a two- to three-fold rise in bulk sediment Ca/Ti, Ba/Ti, and Al/Ti ratios, and a significant increase in the $\delta^{13}C$ gradient of the water column. These observations provide compelling evidence for the biogenic bloom at a frontal zone in the southwest Pacific Ocean. However, manifestations of the biogenic bloom at this location are complex because time offsets occur between various proxies for productivity and between $\delta^{13}C$ records of different carbonate phases. First, $CaCO_3$ MARs peak ca. 5 Ma whereas elemental ratios are highest ca. 6.5 Ma. Second, planktic and benthic foraminifera record the Chron C3AR carbon shift between 7.8 and 6.4 Ma, and between 8.7 and 6.7 Ma, respectively, but bulk sediment does not show this shift (sensu stricto). Although not stressed in previous literature, these time offsets have been documented in other sediment cores from the Indian and Pacific oceans, suggesting underlying causes. At site 590, elemental ratios normalized to Ti are probably affected after 6 Ma because of a significant increase in terrigenous fluxes.

Discrepancies between the $\delta^{13}C$ records of bulk sediment and surface-dwelling planktic foraminifera at site 590 can be explained in terms of different depth habitats of coccolithophores and foraminifera, changes in the rate of upwelling at the TF, and compositional variations in the coccolithophorid assemblage. Together, the biogenic bloom and carbon isotope shifts at site 590 are most readily explained by hydrographic change at the TF affecting nutrient cycling and carbon isotope gradients in the water column.

Acknowledgements

Funding for K.M.G. was supported by a JCU scholarship and through Australian Research Council (ARC) grants to G.R. Dickens and R.M. Carter. We are grateful for the constructive comments of R.W. Murray and an anonymous reviewer. We sincerely thank RMC for his support and comments, Keith Turnbull and Paul Gammon at Adelaide University for stable isotope analyses, and Elvy Grigolato at the JCU-AAC for XRF analyses.

References

Anderson, T.F., Cole, S.A., 1975. The stable isotope geochemistry of marine coccoliths: A preliminary comparison with planktonic foraminifera. J. Foram. Res. 5, 188–192.

Anderson, T.F., Steinmetz, J.C., 1981. Isotopic and biostratigraphical records of calcareous nannofossils in a Pleistocene core. Nature 294, 741–745.

Auzende, J.-M., Dickens, G.R., van de Beuque, S., Exon, N.F., François, C., Lafoy, Y., Voutay, O., 2000. Thinned crust in Southwest Pacific may harbor gas hydrate. EOS Trans. Am. Geophys. Union 81 (182), 185.

Barton, C.E., Bloemendal, J., 1986. Paleomagnetism of sediments collected during Leg 90, Southwest Pacific. Init. Rept. DSDP 90, 1273–1316.

Bé, A.W.H., 1977. An ecological, zoogeographic and taxonomic review of recent planktonic foraminifera. In: Ramsay, A.T.S. (Ed.), Oceanic Micropaleontology. Academic Press, London, pp. 1–100.

Bé, A.W.H., Caron, D.A., Anderson, O.R., 1981. Effects of

feeding frequency on life processes of the planktonic foraminifer *Globigerinoides sacculifer* in laboratory culture. J. Mar. Biol. Assoc. 61, 257–277.

Bé, A.W.H., Tolderlund, D.S., 1971. Distribution and ecology of living planktonic foraminifera in surface waters of the Atlantic and Indian Oceans. In: Funnel, B.M., Riedel, W.R. (Eds.), The Micropaleontology of Oceans, Cambridge University Press, pp. 105–149.

Bemis, B.E., Spero, H.J., Lea, D.W., Bijma, J., 2000. Temperature influence on the carbon isotopic composition of *Globigerina bulloides* and *Orbulina universa* (planktonic foraminifera). Mar. Micropal. 38, 213–228.

Bender, M.L., Graham, D.W., 1981. On late Miocene abyssal hydrography. Mar. Micropal. 6, 451–464.

Berger, W.H., Vincent, E., 1986. Deep-sea carbonates: Reading the carbon isotope signal. Geol. Runds. 75, 249–269.

Berger, W.H., Leckie, R.M., Janecek, T.R., Stax, R., Takayama, T., 1993. Neogene carbonate sedimentation on Ontong Java Plateau: Highlights and open questions. Proc. ODP Sci. Res. 130, 711–744.

Berggren, W.A., Kent, D.V., Van Couvering, J.A., 1985. Neogene geochronology and chronostratigraphy. In: Snelling, N.J. (Ed.), Geochronology and the Geologic Record. Geol. Soc. London Mem. 10, pp. 211–260.

Berggren, W.A. et al., 1995a. Late Neogene chronology: New perspectives in high-resolution stratigraphy. Geol. Soc. Am. Bull. 107, 1272–1287.

Berggren, W.A., Kent, D.V., Swisher, C.C.I., Aubrey, M.-P., 1995. A revised Cenozoic geochronology and chronostratigraphy, In: Geochronology Timescales and Global Stratigraphic Correlation, SEPM Spec. Pub. 54, pp. 212.

Bishop, J.K.B., 1988. The barite-opal-organic carbon association in oceanic particulate matter. Nature 331, 341–343.

Chow, T.J., Goldberg, E.D., 1960. On the marine geochemistry of barium. Geochim. Cosmochim. Acta 20, 192–198.

Ciesielski, P.F., Ledbetter, M.T., Ellwood, B.B., 1982. The development of Antarctic glaciation and the Neogene paleoenvironment of the Maurice Ewing Bank. Mar. Geol. 46, 1–51.

Comiso, J.C., McLain, C.R., Sullivan, C.W., Ryan, J.P., Leonard, C.L., 1993. Coastal zone colour scanner pigment concentrations in the Southern Ocean and relationships to geophysical surface features. J. Geophys. Res. 98, 2419–2451.

Coplen, T.-B., Kendall, C., Hopple, J., 1983. Comparison of stable isotope reference samples. Nature 302, 236–238.

Dehairs, F., Chesselet, R., Jedwab, J., 1980. Discrete suspended particles of barite and the barium cycle in the open ocean. Earth Planet. Sci. Lett. 49, 528–550.

Delaney, M.L., Filippelli, G.M., 1994. An apparent contradiction in the role of phosphorus in Cenozoic chemical mass balances for the world ocean. Paleoceanography 9, 513–527.

Dickens, G.R., Owen, R.M., 1994. Late Miocene-early Pliocene manganese reduction in the central Indian Ocean: Expansion of the intermediate water oxygen minimum zone. Paleoceanography 9, 169–181.

Dickens, G.R., Owen, R.M., 1996. Sediment geochemical evidence for an early-middle Gilbert (early Pliocene) productivity peak in the North Pacific Red Clay Province. Mar. Micropal. 27, 107–120.

Dickens, G.R., Owen, R.M., 1999. The latest Miocene-early Pliocene biogenic bloom: A revised Indian Ocean perspective. Mar. Geol. 161, 75–91.

Diester-Haass, L., Meyers, P.A., Vidal, L., 2002. The late Miocene onset of high productivity in the Benguela Current upwelling system as part of a global pattern. Mar. Geol. 180, 87–103.

Dobson, D.M., Dickens, G.R., Rea, D.K., 2001. Terrigenous sediment on Ceara Rise; a Cenozoic record of South American orogeny and erosion. Palaeogeogr. Palaeoclimatol. Palaeoecol. 165, 215–229.

Drewry, D.J., 1978. Aspects of the early evolution of West Antarctic ice. In: Van Zinderen Bakker, E.M. (Ed.), Antarctic Glacial History and World Palaeoenvironments. A.A. Balkema, Rotterdam, pp. 25–32.

Dudley, W.C., Nelson, C.S., 1989. Quaternary surface-water isotope signal from calcareous nannofossils at DSDP Site 593, Southern Tasman Sea. Mar. Micropal. 13, 353–373.

Dudley, W.C., Nelson, C.S., 1994. The influence of non-equilibrium isotope fractionation on the Quaternary calcareous nannofossil stable isotope signal in the southwest Pacific Ocean, DSDP Site 594. Mar. Micropal. 24, 3–27.

Dudley, W.C., Duplessy, J.C., Blackwelder, P.L., Brand, L.E., Guillard, R.R.L., 1980. Coccoliths in Pleistocene-Holocene nannofossil assemblages. Nature 285, 222–223.

Dudley, W.C., Blackwelder, P., Brand, L., Duplessy, J.-C., 1986. Stable isotopic composition of coccoliths. Mar. Micropal. 10, 1–8.

Dymond, J., 1981. Geochemistry of Nazca Plate surface sediments: an evaluation of hydrothermal, biogenic, detrital, and hydrogenous sources. In: Kulm, L.D. et al. (Eds.), Nazca Plate: Crustal Formation and Andean Convergence. Geol. Soc. Am. Mem., pp. 133–174.

Dymond, J., Suess, E., Lyle, M., 1992. Barium in deep-sea sediment: A geochemical proxy for paleoproductivity. Paleoceanography 7, 163–181.

Elmstrom, K.M., Kennett, J.P., 1986. Late Neogene paleoceanographic evolution of site 590: Southwest Pacific. In: Kennett, J.P., von der Borch, C.C. (Eds.), Init. Repts. DSDP 90, pp. 1361–1381.

Farrell, J.W., Raffi, I., Janecek, T.R., Murray, D.W., Levitan, M., Delaney, M., Dadey, K.A., Emeis, K.-C., Lyle, M., Flores, J.-A., Hovan, S., 1995. Late Neogene sedimentation patterns in the eastern equatorial Pacific. Proc. ODP Sci. Res. 138, 717–756.

Faure, G., 1998. Principles and Applications of Geochemistry. Prentice-Hall, 600 pp.

Filippelli, G.M., 1997. Intensification of the Asian monsoon and a chemical weathering event in the late Miocene-early Pliocene: Implications for late Neogene climate change. Geology 25, 27–30.

Filippelli, G.M., Delaney, M.L., 1995. Phosphorus geochemistry and accumulation rates in the eastern equatorial Pacific Ocean: results from leg 138. Proc. ODP Sci. Res. 138, 757–767.

Gaina, C., Müller, D.R., Royer, J.-Y., Stock, J., Hardebeck, J.L., Symonds, P., 1998. The tectonic history of the Tasman Sea; a puzzle with 13 pieces. J. Geophys. Res. B Sol. Earth Planet. 103, 12413–12433.

Goodney, D.E., Margolis, S.V., Dudley, W.C., Kroopnick, P., Williams, D.F., 1980. Oxygen and carbon isotopes of recent calcareous nannofossils as paleoceanographic indicators. Mar. Micropal. 5, 31–42.

Goldberg, E.D., Arrhenius, G.O.S., 1958. Chemistry of pelagic sediments. Geochim. Cosmochim. Acta 13, 153–212.

Hagino, K., Okada, H., Matsuoka, H., 2000. Spatial dynamics of coccolithophores in the Equatorial Western-Central Pacific Ocean. Mar. Micropal. 39, 53–72.

Haug, G.H., Tiedemann, R., 1998. Effect of the formation of the Isthmus of Panama on Atlantic Ocean thermohaline circulation. Nature 393, 673–676.

Hayes, D.E., Ringis, J., 1973. Seafloor spreading in the Tasman Sea. Nature 243, 454–458.

Heath, R.A., 1985. A review of the physical oceanography of the seas around New Zealand - 1982. New Zealand J. Mar. Freshwater Res. 19, 79–124.

Hermoyian, C.S., Owen, R.M., 2001. Late Miocene–early Pliocene biogenic bloom: Evidence from low-productivity regions of the Indian and Atlantic Oceans. Paleoceanography 16, 95–100.

Jenkins, D.G., Srinivasan, M.S., 1986. Cenozoic planktonic foraminifers from the equator to the subantarctic of the Southwest Pacific. Init. Repts. DSDP 90, 795–834.

Kahn, M.I., 1979. Non-equilibrium oxygen and carbon isotopic fractionation in tests of living planktonic foraminifera. Oceanol. Acta 2, 195–208.

Kahn, M.I., Williams, D.F., 1981. Oxygen and carbon isotopic composition of living planktonic foraminifera from the northeast Pacific Ocean. Palaeogeogr. Palaeoclimatol. Palaeoecol. 33, 47–69.

Kawagata, S., 2001. Tasman front shifts and associated paleoceanogrphic changes during the last 250, 000 years: foraminiferal evidence from the Lord Howe Rise. Mar. Micropal. 41, 167–191.

Keigwin, L.D., 1979. Late Cenozoic stable isotope stratigraphy and paleoceanography of DSDP Sites from the east equatorial and central north Pacific Ocean. Earth Planet. Sci. Lett. 45, 361–382.

Keigwin, L.D., 1982. Isotope paleoceanography of the Caribbean and east Pacific: role of Panama uplift in late Neogene time. Science 217, 350–353.

Keigwin, L.D.J., Aubrey, M.-P., Kent, D.V., 1987. North Atlantic late Miocene stable isotope stratigraphy, biostratigraphy and magnetostratigraphy. Init. Repts. DSDP 94, 935–963.

Kennett, J.P., 1986. Miocene to early Pliocene oxygen and carbon isotope stratigraphy of the Southwest Pacific, DSDP Leg 90. Init. Repts. DSDP 90, 1383–1411.

Kennett, J.P., von der Borch, C.C., 1986. Southwest Pacific Cenozoic paleoceanography. Init. Repts. DSDP 90, 1493–1517.

Kennett, J.P., von der Borch, C.C. et al., 1986. Init. Repts. DSDP 90. U.S. Government Printing Office, Washington, 744 pp.

Kroopnick, P.M., 1985. The distribution of ^{13}C of ΣCO_2 in the world oceans. Deep Sea Res. 32, 57–84.

Lazarus, D. et al., 1992. Revised Chronology of Neogene DSDP Holes from the World Ocean. ODP Technical Note 24, Texas A&M University, TX.

Lohman, W.H., 1986. Calcareous nannoplankton biostratigraphy of the southern Coral Sea, Tasman Sea, and southwestern Pacific Ocean, Deep Sea Drilling Project Leg 90: Neogene and Quaternary. Init. Repts. DSDP 90, 763–793.

Loutit, T.S., Kennett, J.P., Savin, S.M., 1983. Miocene equatorial and southwest Pacific paleoceanography from stable isotopic evidence. Mar. Micropal. 8, 215–233.

Martínez, J.I., 1994. Late Pleistocene palaeoceanography of the Tasman Sea: Implications for the dynamics of the warm pool in the western Pacific. Palaeogeogr. Palaeoclimatol. Palaeoecol. 112, 19–62.

Mead, G.A., Hodell, D.A., Müller, D.W., Ciesielski, P.F., 1991. Fine-fraction carbonate oxygen and carbon isotope results from site 704: implications for movement of the Polar Front during the late Pliocene. Proc. ODP Sci. Res. 114, 437–458.

Moran, S.B., Moore, R.M., 1988a. Evidence from mesocosm studies for biological removal of dissolved aluminum from seawater. Nature 335, 706–708.

Moran, S.B., Moore, R.M., 1988b. Temporal variations in dissolved and particulate aluminum during a spring bloom. Est. Coast. Shelf Sci. 27, 205–215.

Morgans, H.E.G., Scott, G.H., Beu, A.G., Graham, I.J., Mumme, T.C., George, W.S., Strong, C.P., 1996. New Zealand Cenozoic Time Scale (version 11/96). Rep. Inst. Geol. Nucl. Sci. 96/38, 1–12.

Morin, R.H., 1986. Physical properties of calcareous sediments from the southwest Pacific. Init. Repts. DSDP 90, 1239–1246.

Mulhearn, P.J., 1987. The Tasman Front: A study using satellite infrared imagery. J. Phys. Oceanogr. 17, 1148–1155.

Müller, G., Gastner, M., 1971. The 'karbonate bomb', a simple device determination of the carbonate content in sediments, soils, and other materials. Neues Jahr. Mineral. 10, 446–469.

Müller, D.W., Hodell, D.A., Ciesielski, P.F., 1991. Late Miocene to earliest Pliocene (9.8–4.5 Ma) paleoceanography of the Subantarctic Southeast Atlantic: stable isotopic, sedimentologic, and microfossil evidence. Proc. ODP Sci. Res. 114, 459–474.

Murray, D.W., Farrell, J.W., McKenna, V., 1995. Biogenic sedimentation at site 847, eastern equatorial Pacific Ocean, during the past 3 M.Y.. Proc. ODP Sci. Res. 138, 429–459.

Murray, R.W., Leinen, M., 1996. Scavenged excess aluminum and its relationship to bulk titanium in biogenic sediment from the central equatorial Pacific. Geochim. Cosmochim. Acta 60, 3869–3878.

Murray, R.W., Leinen, M., Isern, A.R., 1993. Biogenic flux of Al to sediment in the central equatorial Pacific Ocean: evi-

dence for increased productivity during glacial periods. Paleoceanography 8, 651–670.
Nelson, C.S., 1986. Lithostratigraphy of Deep Sea Drilling Project Leg 90 drill sites in the southwest pacific Ocean: an overview. Init. Repts. DSDP 90, 1471–1491.
Ogg, J., 1998. Digital time scale databases. Mesozoic Stratigraphic Laboratory, Dept. of Earth and Atmospheric Sciences, Purdue University, IN.
Orians, K.J., Bruland, K.W., 1986. The biogeochemistry of aluminum in the Pacific Ocean. Earth Planet. Sci. Lett. 76, 397–410.
Paull, C.K., Thierstein, H.R., 1987. Stable isotopic fractionation among particles in Quaternary coccolith-sized deep-sea sediments. Paleoceanography 2, 423–429.
Peterson, L.C., Murray, D.W., Ehrann, W.U., Hempel, P., 1992. Cenozoic carbonate accumulation and compensation depth changes in the Indian Ocean. In: Duncan, R.A., Rea, D.K., Kidd, R.B., Von Rad, U., Weissel, J.K. (Eds.), Synthesis of Results from Scientific Drilling in the Indian Ocean, Geophysical Monograph 70. American Geophysical Union, pp. 311–333.
Ravelo, A.C., Fairbanks, R.G., 1995. Carbon isotopic fractionation in multiple species of planktonic foraminifera from core-tops in the tropical Atlantic. J. Foram. Res. 25, 53–74.
Raymo, M.E., Ruddiman, W.F., Froelich, P.N., 1988. Influence of late Cenozoic mounain building on ocean geochemical cycles. Geology 16, 649–653.
Rea, D.K., Leinen, M., 1985. Neogene history of the calcite compensation depth and lysocline in the South Pacific Ocean. Nature 316, 805–807.
Savin, S.M., Douglas, R.G., Keller, G., Killingley, J.S., Shaughnessy, L., Sommer, M.A., Vincent, E., Woodruff, F., 1981. Miocene benthic foraminiferal isotope records: A synthesis. Mar. Micropal. 6, 423–450.
Schroeder, J.O., Murray, R.W., Leinen, M., Pflauum, R.C., Janecek, T.R., 1997. Barium in equatorial Pacific carbonate sediment: Terriginous, oxide, and biogenic associations. Paleoceanography 12, 125–146.
Scott, B.D., 1981. Hydrological structure and phytoplankton distribution in the region of a warm-core eddy in the Tasman Sea. Aust. J. Mar. Freshwater Res. 32, 479–492.
Scott, G.H., Bishop, S., Burt, B.J., 1990. Guide to some Neogene Globorotalids (Foraminiferida) from New Zealand, New Zealand Geological Survey Paleontological Bulletin, 61, 135 pp.
Shackleton, N.J., Hall, M.A., 1995. Stable isotope records in bulk sediments (Leg 138). Proc. ODP Sci. Res. 138, 797–805.
Shackleton, N.J., Hall, M.A., 1997. The late Miocene stable isotope record, Site 926. Proc. ODP Sci. Res. 154, 367–373.
Shackleton, N.J., Crowhurst, S., Hagelburg, T., Pisias, N.G., Schneider, D.A., 1995. A new late Neogene timescale: Application to Leg 138 sites. Proc. ODP Sci. Res. 138, 73–101.
Spero, H.J., 1992. Do planktic foraminifera accurately record shifts in the carbon isotopic composition of seawater ΣCO_2? Mar. Micropal. 19, 275–285.
Spero, H.J., Bijima, J., Lea, D.W., Bemis, B.E., 1997. Effect of seawater carbonate concentration on foraminiferal carbon and oxygen isotopes. Nature 390, 497–500.
Spero, H.J., Lea, D.W., 1993. Intraspecific stable isotope variability in the planktic foraminifera *Globigerinoides sacculifer*: results from laboratory experiments. Mar. Micropal. 22, 221–234.
Srinivasan, M.S., Sinha, D.K., 2000. Ocean circulation in the tropical Indo-Pacific during early Pliocene (5.6–4.2 Ma): Paleobiogeographic and isotopic evidence. Proceedings of the Indian Academy of Sciences–Earth & Planetary Sciences, 109, 315–328.
Stein, R., Robert, C., 1986. Siliclastic sediments at Sites 588, 590, and 591: Neogene and Paleogene evolution in the southwest Pacific and Australian climate. Init. Repts. DSDP 90, 1437–1455.
Tilburg, C.E., Hurlburt, H.E., O'Brien, J.J., Shriver, J.F., 2001. The dynamics of the East Australian Current system: the Tasman Front, the East Auckland Current, and the East Cape Current. J. Phys. Oceanogr. 31, 2917–2943.
Uddstrom, M.J., Oien, N.A., 1999. On the use of high-resolution satellite data to describe the spatial and temporal variability of sea surface temperatures in the New Zealand region. J. Geophys. Res. 104, 20729–20751.
Van Andel, T.H., 1975. Mesozoic/Cenozoic calcite compensation depth and the global distribution of calcareous sediments. Earth Planet. Sci. Lett. 26, 187–194.
Van Andel, T.H., Heath, G.R., Moore Jr., T.C., 1975. Cenozoic history and paleoceanography of the central equatorial Pacific Ocean: a regional synthesis of Deep Sea Drilling project data. Geol. Soc. Am. Mem. 143, 143 pp.
Vergnaud-Grazzini, C., 1976. Non-equilibrium isotopic compositions of shells of planktonic foraminifera in the Mediterranean Sea. Palaeogeogr. Palaeoclimatol. Palaeoecol. 20, 263–276.
Vincent, E., Killingley, J.S., Berger, W.H., 1980. The magnetic epoch 6 carbon shift: A change in the ocean's $^{13}C/^{12}C$ ratio 6.2 million years ago. Mar. Micropal. 5, 185–203.
Vincent, E., Killingley, J.S., Berger, W.H., 1985. Miocene oxygen and carbon isotope stratigraphy of the tropical Indian Ocean. Geol. Soc. Am. Mem. 163, 103–130.
Warren, B.A., 1970. General circulation in the South Pacific. In: Wooster, W.S. (Ed.), Scientific Exploration of the South Pacific. National Academy of Sciences, Washington, DC, pp. 33–49.
Willcox, J.B., Symonds, P.A., Hinz, K., Bennett, D., 1980. Lord Howe Rise, Tasman Sea - preliminary geophysical results and petroleum prospects. BMR J. Aust. Geol. Geophys. 5, 225–236.
Williams, D.F., Sommer II, M.A., Bender, M.L., 1977. Carbon isotopic compositions of recent planktonic foraminifera of the Indian Ocean. Earth Planet. Sci. Lett. 36, 391–403.
Wright, I.C., Vella, P.P., 1988. A New Zealand late Miocene magnetostratigraphy: glacioeustatic and biostratigraphic correlations. Earth Planet. Sci. Lett., 87, 193–204.